THE PENNSYLVANIA STATE UNIVERSITY

SCHREYER HONORS COLLEGE

DEPARTMENT OF ENGINEERING SCIENCE

ULTRASONICS FOR HEALTH MONITORING OF MODEL HUMAN BONES: NUMERICAL APPROACH

COLIN SLAVTCHEFF

SPRING 2021

A thesis
submitted in partial fulfillment
of the requirements
for a baccalaureate degree
in Engineering Science and Mechanics
with honors in Engineering Science
Reviewed and approved* by the following:

Dr. Clifford Lissenden, PhD

Professor of Engineering Science and Mechanics, Acoustics

Thesis Supervisor

Dr. Lucas Passmore, PhD

Associate Professor of Engineering Science and Mechanics

Honors Academic Advisor

Dr. Judith A. Todd, PhD

Department Head

P.B. Brenneman Chair

Professor of Engineering Science and Mechanics

*Signatures are on file in the Schreyer Honors College and in the ESC office.

*Electronic approvals are on file.

Technical Abstract

Bone characterization using Quantitative Ultrasound (QUS) is an attractive alternative to x-ray techniques in cases such as monitoring fracture healing and management of osteoporosis, due to its non-ionizability, portability, and lower cost. Investigated in this paper is the characterization of ultrasonic wave propagation through waveguides with bone-like properties. Physical experiments are performed in a companion thesis on two waveguides: plate and pipe. Simulations designed to recreate these physical experiments are used to provide greater understanding of the results. Both experiments yielded amplitude-time data for equidistant points along the model. Waveform characterization, group velocity, and attenuation rate can be found for each geometry at different frequencies with different material properties. Progress has been made in waveform analysis for ultrasound in bone-mimicking material.

Non-Technical Abstract

In recent years, ultrasonic guided waves have gained traction in the medical field as a characterization tool for bones. Bone ultrasound can be used to detect and monitor fractures as well as give an indication of bone health. This research simulates propagation of ultrasonic waves through plate and pipe models with bone properties. The data collected from the simulations is then compared to data from experiments performed on physical models.

TABLE OF CONTENTS

LIST OF FIGURES

LIST OF TABLES

Acknowledgements

For his patient guidance and sage advice I would like to thank Dr. Clifford Lissenden. Without his deep knowledge of the ultrasonics field, my understanding of its central concepts would be severely lacking. I would like to thank Anurup Guha, our resident graduate student, for jumping in the trenches with us and showing us how it's done. Without Mr. Guha, I would have never successfully created a simulation in ABAQUS. Finally, my fellow undergraduate researcher, Tyler Duane, gave me encouragement and reassurance during the greatest struggles of completing our theses.

CHAPTER 1
INTRODUCTION

PROBLEM STATEMENT

Demand for the characterization of bone using ultrasonics is expanding thanks to its various capabilities, including:

1. Management of complex bone healing processes[1]
2. Ability to diagnose bone fractures[2]
3. Increases accuracy in Osteoporosis diagnosis[3]
4. Increases accessibility of bone testing equipment[4]

In almost all cases, bone assessment and fracture detection is achieved by x-ray techniques[5]. For example, Dual-Xray Absorptiometry (DEXA) is used when measuring bone density for osteoporosis. These X-Ray methods send ionizing radiation into the body to assess bone quality. Radiation in our bodies can cause harmful cell mutations, leading to cancer. Thus, radiation should be avoided when possible. In addition, techniques like DEXA require expensive equipment, driving up procedure costs.

Ultrasound has a number of benefits: it does not involve ionizing radiation, it is noninvasive, it can determine material properties as well as detect discontinuities, it uses equipment that is portable so it can be done in the field or office as opposed to a dedicated facility, and it is relatively inexpensive[4].

Ultrasound will be investigated as an informational tool for healthcare workers as they manage the bone healing process. Open questions include what type of waves to send, what transducers to use, and how to process the data. Our research hopes to lay the groundwork to prove the efficacy of ultrasound in managing bone fracture healing.

DESIGN NEEDS

The materials used in this research include:

- ABAQUS modeling software
- 5th metatarsal CT scan
- SolidWorks
- FiberTuff™ 3D Printing Material

The design aspect in this research centers on the building of models in ABAQUS finite element analysis software. This includes designing the boundary conditions, mesh, and output parameters of the simulations.

Public Health

Before actualizing a technological breakthrough, much supporting data is needed to refine the technology and theory. Many 5th metatarsal fractures, especially the one known as a Jones Fracture, are common sites of delayed union and non-union due to the poor blood flow in the area[6]. As a result, multiple check-ups are required during the healing process to ensure proper bone fusion. Because of ultrasound's non-ionizing radiation, frequency of testing is not a safety concern, therefore the healing process can be more closely monitored and complications corrected more swiftly. Of course, the findings of this research could be extended to any other bone of interest and the public would enjoy the cost and safety benefits that ultrasound has over traditional X-Ray methods.

Ethics

The research completed for this project must be as accurate and meticulous as possible, considering the experimental results could be used as the basis in bone health assessments.

Safety considerations

Unlike its X-Ray counterparts, ultrasound techniques are generally considered safe due to its lack of ionizing radiation; the reason it is preferentially used for imaging during pregnancy.

Economic Factors

Ultrasonic equipment is relatively less expensive than imaging technology currently in use. If reliable testing can be performed using bone ultrasonics, it can be a more affordable alternative to current imaging techniques[4].

Global Factors

From arctic research teams to naval submarine crews, personnel in remote locations who suffer a potential bone fracture will have to be evacuated to a nearby medical center with X-Ray capability. Due to its portability, ultrasonic equipment can be brought into remote locations for on-site fracture diagnosis. For those living in remote, resource-deficient areas, ultrasonic equipment makes diagnostic capability an option due to its affordability compared to X-Ray equipment. These two factors, portability and affordability, will make fracture diagnosis more accessible on a global scale[4].

Objectives of Thesis

Wave propagation is to be characterized for bone waveguides of different geometries to obtain damping and identify wave modes. Comparison of excitation frequencies and material properties for ultrasound in bone will be conducted.

CHAPTER 2
LITERATURE REVIEW

INTRODUCTION

Similar to how Ultraviolet light is outside the visible spectrum for humans, ultrasonic sound encompasses the sound wave frequencies above the upper limit of human hearing[7]. These frequencies start at 20 kHz and climb until they reach the hypersonic zone past 1 GHz[7]. The discovery of the piezoelectric effect in 1880 has led to the development of the piezoelectric transducer, a fine piece of technology that allows ultrasonic waves to be produced and received. There are many different types of waves, also called wave modes, that can be produced, but the main ones are: longitudinal, transverse (shear), surface (Rayleigh), and plate (Lamb)[7]. These modes can be further categorized as either *bulk* or *guided*[7]. The selection of wave type (or types) for any particular application depends on the test piece's geometry and material properties[7].

Thanks to technological advancement in the past few decades (mainly here at Penn State), guided waves have become a more understood and available technology[5]. Guided waves rely on the test piece to act as a wave guide, using its natural boundaries to guide the wave propagation along its length[7]. Shown in Figure 1 is a comparison of the two techniques.

FIGURE 1: PROPAGATION COMPARISON OF BULK VS GUIDED WAVES [8]

Guided waves have a number of specific advantages over bulk waves. For one, guided waves can reach further into a test piece, which means you don't need direct access to the area you are evaluating and you don't have to be as precise with your transducer placement[7]. For these reasons, guided waves are gaining traction as the preferred method of wave propagation.

For the most part, ultrasonic waves have been used for material testing and characterization, a rapidly-growing field known as Ultrasonic Testing (UT), under the larger umbrella of Nondestructive Evaluation (NDE) and Structural Health Monitoring (SHM). Attention towards using sound waves as a long range detection method was first sparked after the 1912 Titanic disaster when a patent for detecting underwater icebergs was filed [9]. Further advances in this area were made by Allied forces in WW1 in attempts to detect German U-Boat submarines, resulting in SONAR technology. Such advances eventually led to the ultrasonic testing systems used today.

The ultrasonic testing market is growing, with an expected valuation of $3.93 billion by the year 2022[10]. Modern applications in the ultrasonic testing field include medical ultrasound, flaw detection in materials manufacturing, testing for pipe corrosion, measuring material thickness, and testing for cracks and defects in metal parts. The list of applications is constantly expanding as research unveils different ways to manipulate ultrasonic waves and unlock hidden potential. One such area of potential is Bone Ultrasonics[11].

BONE ULTRASONICS

Bones serve as the load bearing architecture in the body. There are two components to bone: cortical and cancellous. Cortical bone refers to the hard, low-porosity external shell of all bones and is denser than cancellous bone. Cancellous bone, sometimes referred to as spongy or trabecular bone, makes up the porous inner bone material. These two bone types have different mechanical properties such as Young's Modulus, Poisson's Ratio, and Shear Modulus, to name a few. Ultrasonic Testing (UT) techniques have found footing in recent years as a promising diagnostic and measurement tool for bone degradation such as Osteoporosis and fracture. This subset of ultrasonic testing as it relates to bones is known as Quantitative Ultrasound (QUS)[1].

Osteoporosis is a condition in which the body does not produce enough bone material to keep up with the body's natural bone material removal, often resulting in fracture. There are over 8.9 million fractures annually due to osteoporosis, resulting in enormous economic and well-being costs.[12] Currently, osteoporosis is diagnosed according to measurements using Dual X-Ray Absorptiometry (DXA)[5]. DXA is used as a diagnostic tool by measuring the Bone

Mineral Density (BMD) in the hip or spine and assigning to this measurement a “T-Score”. The T-score is the number of standard deviations from “healthy” BMD measurements. During testing, the BMD is derived from the amount of attenuation experienced by X-rays as they travel through the mineral part of the bone[13].

Early detection of osteoporosis is key in avoiding later fractures, but the higher cost and lower availability of DXA equipment discourages frequent screenings. Utilizing QUS as a screening tool is promising, but the efficacy of QUS in diagnosing osteoporosis has been proven in only one testing location: the calcaneus or heel bone[13]. This result, however, was only tested for some populations, with strongest evidence for Caucasian females over 55 years old.[13] One glaring issue with QUS is the variability between QUS measurement devices, specifically the problem with having to adjust the T-score cutoff for being considered osteoporotic ($T < -2.5$), depending on device and population. To illustrate this problem, in one study[3], different ultrasonic devices classified the percentage of the population of 60 year old women as being osteoporotic from 4% to 50%. Until these problems are worked out and a more effective QUS tool for osteoporosis screening is available, DXA will remain the gold standard for osteoporosis diagnosis.

When a fracture occurs, the bone undergoes a well-defined healing process until the original strength and mechanical properties are restored. In some cases, between 5 and 10%, fractures will not heal properly or at all, extending the healing time on top of the amount of time it already took to realize there was a complication. In these situations where frequent tests are required, QUS is a convenient alternative to the ionizing and costly X-Ray procedure.

In addition to their use in monitoring fracture healing, ultrasonic waves can be used for fracture detection as well[11]. In remote areas such as on Naval ships, in space, in submarines, etc., X-Ray machines are impractical due to their size and weight[2]. The portability of ultrasound devices would allow fracture diagnosis where X-Ray would be impractical. So far, QUS has been able to detect fractures of the clavicle, orbit, foot, ankle, femur, rib, and humerus[2]. In long bones, the most common method for detecting and monitoring fractures is the axial transmission (AT) method, shown in Figure 2.

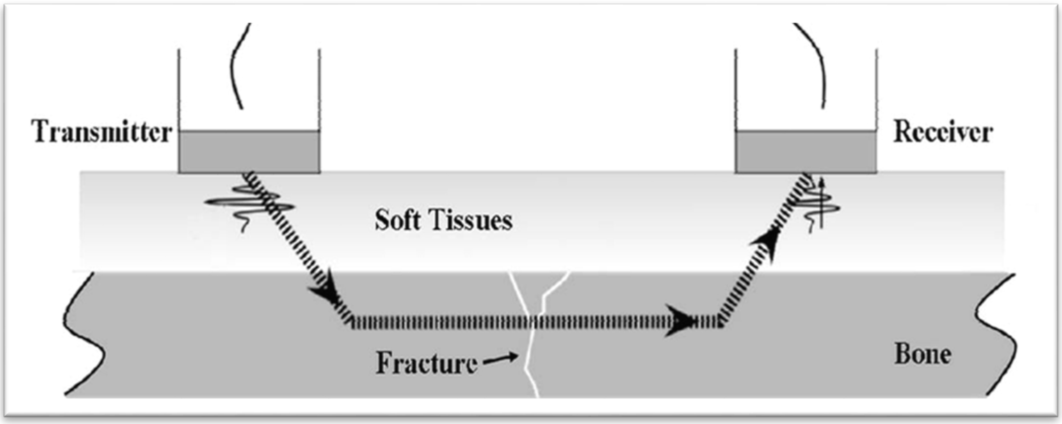

FIGURE 2: AXIAL TRANSMISSION METHOD FOR FRACTURE MONITORING[11]

In the AT method, a transmitter and receiver are placed on either side of the fracture location, on the same side of the bone. The goal is to measure the arrival time of the wave from the transmitter to the receiver. From arrival time, or time of arrival (TOA), one can calculate the velocity of the first arriving signal (FAS) by dividing distance between transducers by time of arrival (TOA)[11]. This gives the speed of sound (SOS) of the wave. Since the bone properties of a healing fracture differ from that of intact cortical bone, the SOS of the wave as it propagates through each scenario is noticeably different. The main properties derived from these tests are speed of sound (SOS) and broadband ultrasound attenuation (BUA)[13].

GUIDED WAVES IN BONES

When guided waves interact with whatever waveguide they are propagating through, their wavelengths will change to adapt to the size of the waveguide at a given frequency[7]. This results in a wide range of modes with their own frequency-dependent phase and group velocities. These wave modes linearly combine to form the elastic wave propagation in the waveguide[7]. Certain wave modes may be more suitable for propagation in a specific medium. Selectively choosing a certain wave mode can be accomplished with transducer design. Dispersion curves plot the propagating wave modes with their velocities (either group or phase) as a function of excitation frequency or excitation frequency times thickness.

Human cortical long bones can be used as ultrasonic waveguides as they are essentially hollow pipes[2]. The Tibia is one such bone, shown from different viewpoints in Figure 3. The Tibia, also known as the shinbone, has a triangular cross-section that varies in shape along its length. Towards either end of the bone the geometry becomes complex, but in the middle of the bone, the mid-diaphysis region, the cross-section geometry is relatively stable[5]. There is also very little soft tissue above the bone in this area, making it an ideal spot for noninvasive transducer placement.

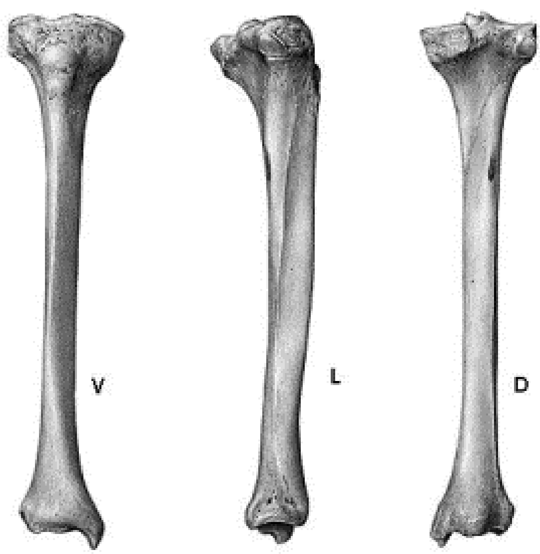

FIGURE 3: TIBIA BONE FROM THREE DIFFERENT ANGLES[14]

A Penn State study[15] from November of 2020 investigated the mid-diaphysis of the Tibia as a potential waveguide. A synthetic composite of the Tibia with properties representing cortical bone is used. For the excitation, an omni-directional shear transducer is used at a lower frequency of 200 kHz in order to minimize attenuation, given the lossy nature of cortical bone's properties. The results of this study showed that ultrasonic guided waves could be detected via displacement measurements at distances between 45 - 85mm. This study put forth evidence that guided waves could propagate to a useful extent in the Tibia, enabling future studies on fracture diagnosis to take place.

THE FIFTH METATARSAL

The fifth metatarsal is a common site for fractures to occur, making up 70% of the metatarsal fractures every year.[6] Typically, these fractures are screened with plain film radiography because of its high specificity (94%), meaning it is effective in determining when there is not a fracture. However, this method has a low sensitivity (10-20%) when it comes to verifying there is a stress fracture, which is why other procedures with high sensitivities such as MRI are used to confirm a positive diagnosis.[6] In one case study, Ultrasonic methods have been proposed as a follow-up procedure for negative radiological results in the hopes of detecting fractures of the fifth metatarsal. A 68 year old woman experiencing foot pain is given a negative diagnosis after radiography, but stress fractures are suspected. Using a linear array transducer operating between 8 - 15 MHz, cortical disruption was observed in the ultrasound imaging, supporting suspected fracturing. CT scans confirmed suspicions of fracture. Four ultrasonic follow-up sessions over the course of three months successfully monitored the healing progress of the bone.

The fracture classification of the fifth metatarsal depends on its location in the bone. Figure 4 illustrates the different fracture zones in the proximal diaphysis of the fifth metatarsal.

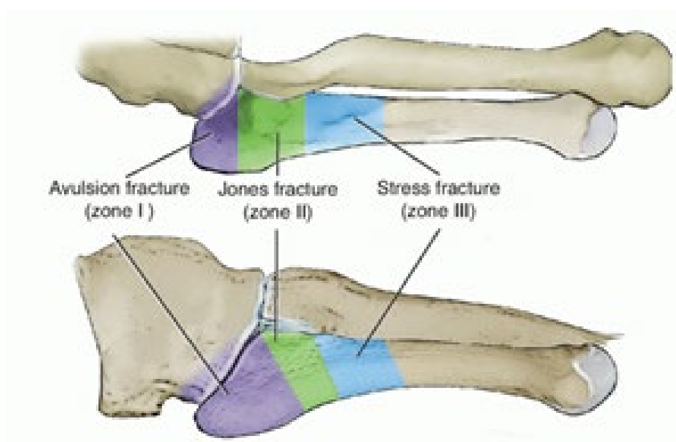

FIGURE 4: FRACTURE ZONES OF 5TH METATARSAL[16]

Fractures in Zone 1, at the base of the metatarsal, are known as Avulsion fractures[17]. Those in Zone 2 towards the middle are called Jones fractures[17]. Zone 3, the furthest away from the base are just called Stress fractures[17]. The Jones Fracture is caused by repetitive weight-bearing and twisting of the foot with high occurrence in sport-related activities. Poor blood supply to the area of the proximal diaphysis is the reason for high frequency of delayed union and non-union of the fracture[17]. A Swedish study conducted over a 5-year period found that out of 66 fifth-metatarsal fractures, one-fourth of fractures treated non-surgically had to be treated surgically later because of delayed union or refracture.[17]

The case study described earlier made use of a linear array transducer, sending bulk waves into the bone. In our research, guided waves will be used to assess properties and detect fractures in the fifth metatarsal.

BONE COMPUTER MODELING

Finite element analysis (FEA) software has been designed to solve the partial differential equations that mathematically describe physical phenomena such as a force applied to a mechanical structure or sound waves propagating through a bone. Since these partial differential equations as they relate to the whole structure are numerically unsolvable with analytical methods, the structure is discretized into smaller parts each with its own defining equations. Finite Element Modeling (FEM) is based on the mathematics of FEA. Before the 1990's, ultrasonic testing on bones required the physical experimentation of *in vivo* or *in vitro* bones, an inherently resource and time consuming process[18]. Another resource and time consuming process is determining the optimal transmission-reception signal parameters for a system, including the frequency, bandwidth, and signal shape to use as well as transducer size, shape, and location[18]. With FEA simulations, bone characteristics and features can easily be changed, quickly modeling complex experiments, some of which would be impossible to physically perform[18].

An application of Finite Element Modeling to estimate cortical thickness in 20 radial bone samples is detailed in a 2008 study. Simulations of ultrasonic propagation from the left side of the radial cross section to a receiver on the opposite side were used to find the net time delay (NDT) for each sample. NDT is the difference in time arrival of the wave with and without the bone in the way. It was found to be an accurate estimation of cortical thickness.[18]

In a more recent 2020 study[15], the Tibia bone is being optimized for ultrasonic wave propagation. Ultrasonic simulation is first used to find the phase velocity dispersion curve for a 2D cross section of the Tibia. A dynamic simulation for experimental validation purposes modelling an omni-directional shear transducer yielded displacement waveforms at the same measurement spot in the physical experiment.

There is strong support for the utility of finite element simulations in ultrasonic bone experiments, both as a tool for experimental optimization and verification[18].

CONCLUSION

Guided waves are a promising tool in the field of non-destructive evaluation, which is a rapidly growing market. The need for cheaper and non-ionizing bone evaluation has led to the investigation of ultrasonics for osteoporosis and fracture detection. Guided waves, known as axial transmission in bones, are being evaluated for fracture detection and healing monitoring with the assistance of finite element modeling.

CHAPTER 3
COMPUTATIONAL METHODS

FINITE ELEMENT THEORY

When ultrasonic waves pass through a material they exert mechanical forces due to the inherent, alternating pressure field of the sound waves. ABAQUS was the primary finite element analysis software used for this research. ABAQUS relies on the Finite Element Method (FEM) to perform Finite Element Analysis (FEA)[19]. To solve for the stresses, strains, and displacements of a continuous system, the FEM goes through the following steps:

1. **Discretize**: divide the continuous system into smaller pieces, known as elements

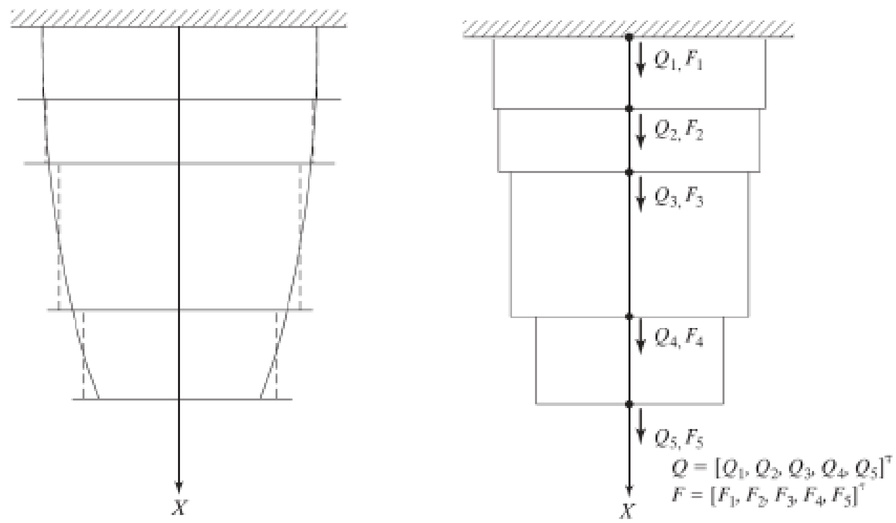

FIGURE 5: DISCRETIZATION OF CONTINUOUS SYSTEMS INTO ELEMENTS[19]

2. **Describe the element connectivity at nodal points**
   The resultant displacements will be found at each node (**U1,U2**). Every element type has a certain number of nodes, e.g. four nodes for a rectangular element[19].

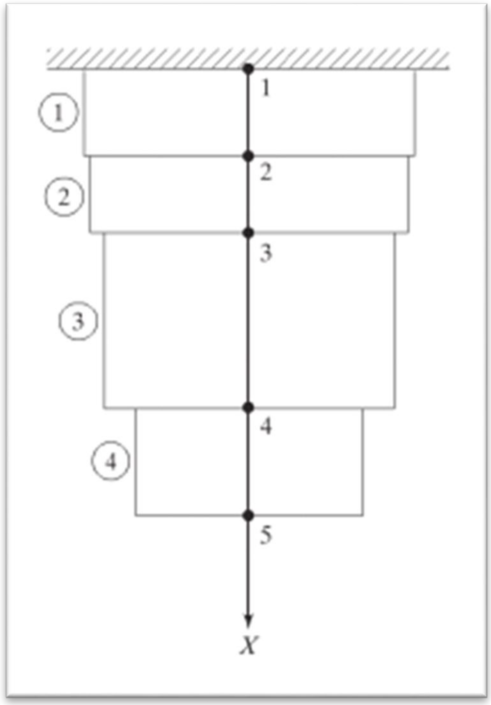

FIGURE 6: NUMBERING OF ELEMENTS AND THEIR NODES[19]

From Figure 6, the following connectivity table can be generated.

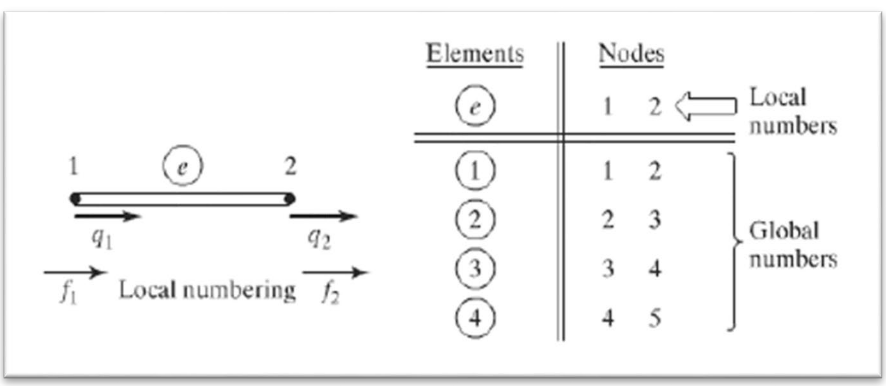

FIGURE 7: ELEMENT-NODE CONNECTIVITY TABLE[19]

3. Describe **element behavior locally** in terms of nodal variables with the following force equation:

$$\underline{m}\underline{\ddot{q}} + \underline{k}\underline{q} = \underline{f}$$

where

$\underline{m}$ = element mass matrix

$\underline{k}$ = element stiffness matrix

$\underline{q}$ = element displacement vector

$\underline{f}$ = element force vector

4. Assemble element equations to obtains global system of equations:

$$\underline{M}\underline{\ddot{Q}} + \underline{K}\underline{Q} = \underline{F}$$

5. Apply boundary conditions including constraints and loads
6. Solve the global system of equations for the global Q matrix
7. Process further to find secondary variables including stress (σ), strain (ϵ), etc.

Where $\underline{q}$ refers to the nodal displacement of an element, $\underline{u}$ is the displacement field inside the element. A shape function matrix, $\underline{N}$, is used to find $\underline{u}$ from $\underline{q}$:

$$\underline{u} = \underline{N}\underline{q}$$

From $\underline{u}$, strain matrix ($\underline{\epsilon}$) can be found from:

$$\underline{\epsilon} = \underline{L}\underline{u} = \underline{L}\underline{N}\underline{q} = \underline{B}\underline{q}$$

From $\underline{\epsilon}$, the stress matrix ($\underline{\sigma}$) can be found from:

$$\underline{\sigma} = \underline{D}\underline{\epsilon} = \underline{D}\underline{B}\underline{q}$$

Element behavior can be described by first defining the Lagrangian of the structure undergoing FEA and then using Hamilton's Principle to evaluate the Lagrangian, from which the matrices in step 3 can be written explicitly. The Lagrangian, L, is the difference between the kinetic energy and potential energy of the system:

$$L = T - \Pi$$

where

$$T = \frac{1}{2}\int_V \underline{\dot{u}}^T \underline{u}\, p\, dV = \text{Kinetic Energy}$$

$$\Pi = \frac{1}{2}\int_V \underline{\sigma}^T \underline{\epsilon}\, dV - \int_V \underline{u}^T\, \underline{b}\, dV - \int_S \underline{u}^T \underline{T}\, dS = \text{Potential Energy}$$

Hamilton's Principle makes use of the Lagrangian to yield the following relation:

$$\frac{d}{dt}\left(\frac{2L}{2\dot{q}_i}\right) - \frac{2L}{2q_i} = 0$$

q_i are generalized variables. The Lagrangian for each element is given by:

$$L_e = \frac{1}{2}\underline{\dot{q}}^T \int_{V_e} \underline{N}^T \underline{N}\, p\, dV\, \underline{\dot{q}} - \frac{1}{2}\underline{q}^T \int_{V} \underline{B}^T \underline{DB}\, dV\, \underline{q} + \underline{q}^T \int_{V_e} \underline{N}^T \underline{b}\, dV + \underline{q}^T \int_{l_e} \underline{N}^T \underline{T}\, dl$$

Inserting the above L_e as L in Hamilton's Principle:

$$\underbrace{\int_{V_e} (\underline{N}^T \underline{N}\, p\, dV)}_{\underline{m}}\, \underline{\ddot{q}} + \underbrace{\int_{V_e} (\underline{B}^T \underline{DB}\, dV)}_{\underline{k}}\underline{q} = \underbrace{\int_{V_e} \underline{N}^T \underline{b}\, dV + \int_{l_e} \underline{N}^T \underline{T}\, dl}_{\underline{f}}$$

Hamilton's Principle describes the behavior for each element, which can be assembled into a global system of equations that represents the entire structure:

$$\underline{m}\underline{\ddot{q}} + \underline{k}\underline{q} = \underline{f} \rightarrow \underline{M}\underline{\ddot{Q}} + \underline{K}\underline{Q} = \underline{F}$$

Simulation Procedure

The simulations completed in ABAQUS are meant to mirror physical experiments completed in the lab. Physical experiments rely on synthetic bone waveguides to approximate bone material properties. Since we had access to the properties of actual cortical bone, these were used within the Abaqus simulation. Both isotropic and anisotropic values are used.

Mass density of cortical bone:

$$\text{Mass Density} = 1930\, \frac{kg}{m^3}$$

Damping factors for cortical bone as a function of frequency:

Table 1: Damping Constant for Cortical Bone

	200 kHz	**500 kHz**
Beta β	$7.5\ x\ 10^{-8}$	$3.18\ x\ 10^{-8}$

For isotropic properties, Young's Modulus (E) and Poisson's Ratio (v) are found from the Generalized Hooke's Law equations:

$$\epsilon_x = \frac{1}{E}[\sigma_x - v(\sigma_y + \sigma_z)]$$
$$\epsilon_y = \frac{1}{E}[\sigma_y - v(\sigma_x + \sigma_z)]$$
$$\epsilon_z = \frac{1}{E}[\sigma_z - v(\sigma_x + \sigma_y)]$$

For anisotropic materials, E and v are combined to form a stiffness matrix (C). The stiffness matrix relates the stress and strain for each principal direction in a material. Figure 8 shows how the C matrix organizes the anisotropic stiffness tensors.

$$\begin{Bmatrix} \sigma_{11} \\ \sigma_{22} \\ \sigma_{33} \\ \sigma_{23} \\ \sigma_{13} \\ \sigma_{12} \end{Bmatrix} = \begin{bmatrix} C_{1111} & C_{1122} & C_{1133} & C_{1123} & C_{1113} & C_{1112} \\ & C_{2222} & C_{2233} & C_{2223} & C_{2213} & C_{2212} \\ & & C_{3333} & C_{3323} & C_{3313} & C_{3312} \\ & & & C_{2323} & C_{2313} & C_{2312} \\ & \iddots & & & C_{1313} & C_{1312} \\ sym & & & & & C_{1212} \end{bmatrix} \begin{Bmatrix} \varepsilon_{11} \\ \varepsilon_{22} \\ \varepsilon_{33} \\ 2\varepsilon_{23} \\ 2\varepsilon_{13} \\ 2\varepsilon_{12} \end{Bmatrix}$$

FIGURE 8: ANISOTROPIC STIFFNESS MATRIX [20]

The stiffness coefficients (C_{ijkl}) for the anisotropic bone material used in simulations is displayed below in Table 2:

TABLE 2: ANISOTROPIC BONE STIFFNESS COEFFICIENTS

Stiffness Coefficient	**Value (GPa)**
C_{1111}	18.37
$C_{2222} = C_{3333}$	8.75
C_{2323}	3.6
$C_{1313} = C_{1212}$	3.3
$C_{1122} = C_{1133}$	3.94
C_{2233}	4.4

All other values are zero.

Element Size

The dispersion curves for anisotropic bone through a plate waveguide, seen in Figure 9, is used to find the largest element size that can be used without losing accuracy.

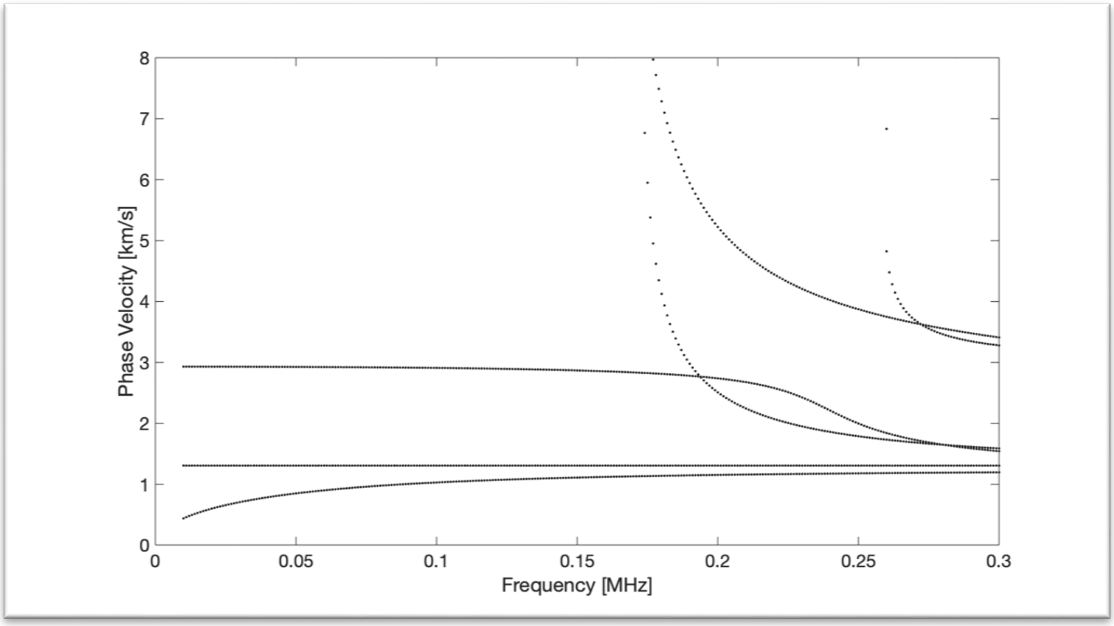

Figure 9: Dispersion Curves for Bone[15]

In the case of both 200 and 500 kHz excitation, the slowest wave speed is 1 km/s and can be used to find the wave's wavelength according to the following relation:

$$\lambda = \frac{c}{f}$$

Equation 1

Then, the largest element size that can be used accurately is found by:

$$largest\ e_{size} = \frac{\lambda}{10}$$

Equation 2

The following table shows wavelength and largest element size for both frequencies.

TABLE 3: LARGEST ELEMENT SIZE FOR EXCITATION FREQUENCY

	$frequency$ (kHz)	
	200	***500***
Wavelength, λ	0.005	0.002
Largest e_{size} (m)	0.0005	0.0002

THEORETICAL GROUP VELOCITIES

The theoretical group velocities for the modes present at each frequency can be found from the dispersion curve for each geometry with bone-like properties. The dispersion curves for plate and pipe are shown in Figure 10.

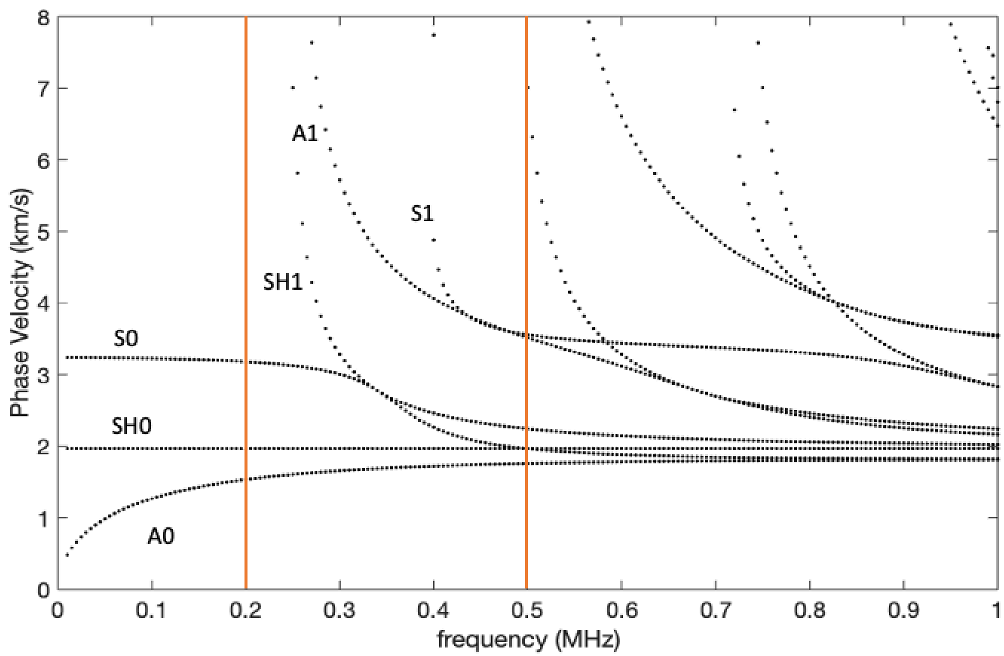

(a)

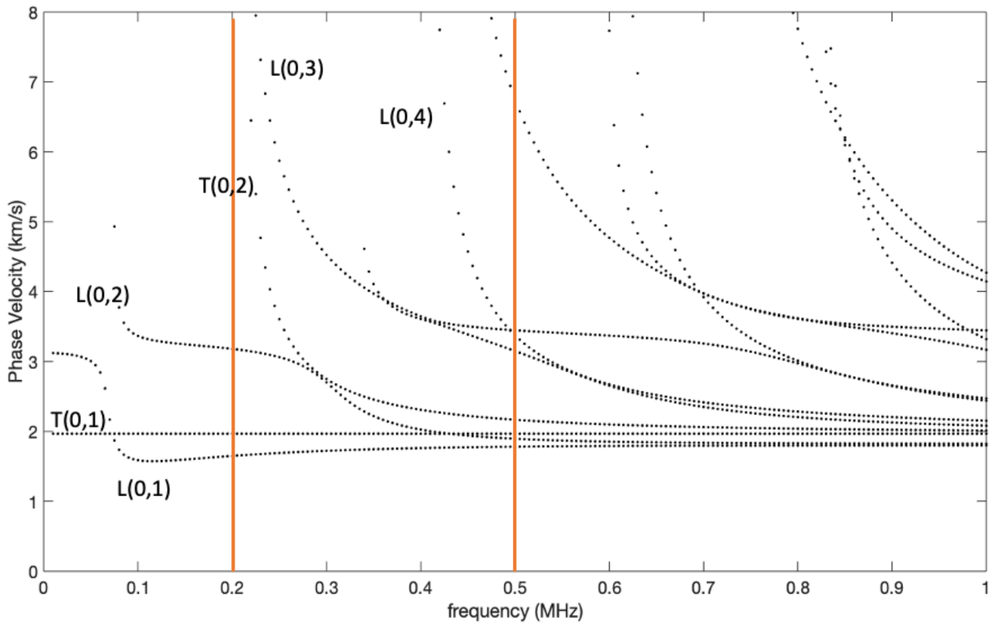

(b)

FIGURE 10: BONE DISPERSION CURVES FOR (A) PLATE GEOMETRY AND (B) PIPE GEOMETRY

If a straight vertical line is drawn at each frequency, shown as orange lines in Figure 10, it would intersect with a number of curves, each representing a wave mode. The theoretical group velocity for these wave modes at a frequency can be calculated from the following equation:

$$v_g = v_p^2 \left[v_p - f \frac{d(v_p)}{d(f)} \right]^{-1}$$

EQUATION 3

where v_p is the y-valued phase velocity and f is the x-valued frequency. The calculation is performed for every mode at 200 and 500 kHz, for each geometry.

Table 4 displays the theoretical group velocities resulting from these calculations.

TABLE 4: THEORETICAL GROUP VELOCITIES

	Group Velocity (km/s)	
Geometry	**200 kHz**	**500 kHz**
Plate	A0 Mode: 1.9708	Mode 1: 1.9086
	SH0 Mode: 1.9680	Mode 2: 1.5545
	S0 Mode: 3.0249	Mode 3: 1.9626
		Mode 4: 1.7269
		Mode 5: 2.2065
		Mode 6: 2.7811
Pipe	L01 Mode: 1.8520	L(0,1) : 1.8544
	T01 Mode: 1.9680	L(0,2) : 1.6071
	L02 Mode: 2.9069	T(0,1) : 1.9625
		T(0,2) : 1.7843
		L(0,3) : 1.7701
		L(0,4) : 1.1474
		Mode 7: 3.3983

SIMULATED WAVE PROPERTIES

Wave properties for the 200 and 500 kHz excitations are listed in the table below.

TABLE 5: SIMULATED WAVE PROPERTIES

# of Wave Cycles	8 cycles, 1 toneburst
Excitation Duration	250 μs
Time step	$5x10^{-8}\ s$

PLATE

The plate geometry must be sketched in the ABAQUS software. The physical dimensions of the plate used for experiments can be seen below in Figure 11.

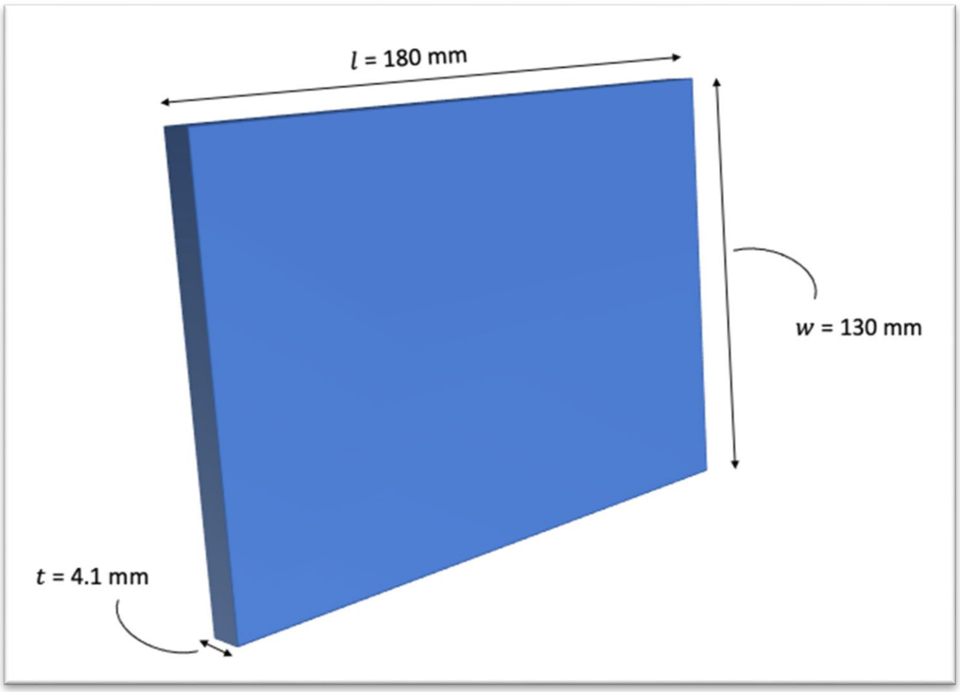

FIGURE 11: PLATE DIMENSIONS

MODEL SIMPLIFICATION AND EXCITATION

In ABAQUS, the 3D plate's geometry can be simplified to a 2D rectangle due to the uniform response that would occur across the width of the plate for every point along the length. The plane strain condition is assumed. The ultrasonic excitation (shown as orange arrows) is positioned on the left edge of the plate with propagation occurring down the length. This setup is shown below in Figure 12.

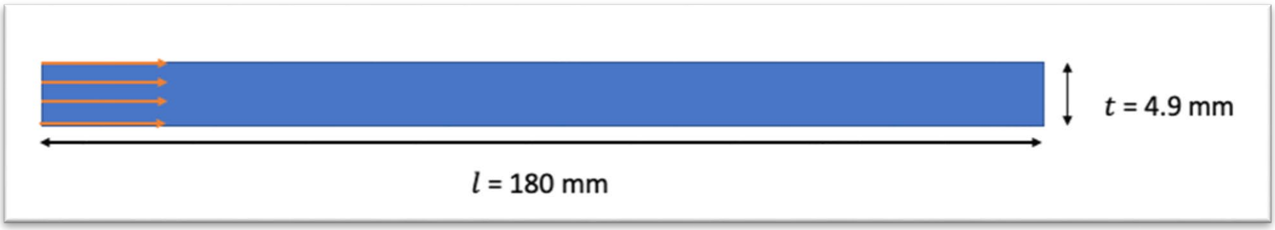

FIGURE 12: 2D MODEL SIMPLIFICATION

MESH

Due to the models' simple geometry, Quadrilateral type elements with 4 nodes are used. The 2D plate mesh composed of these elements is shown in Figure 13.

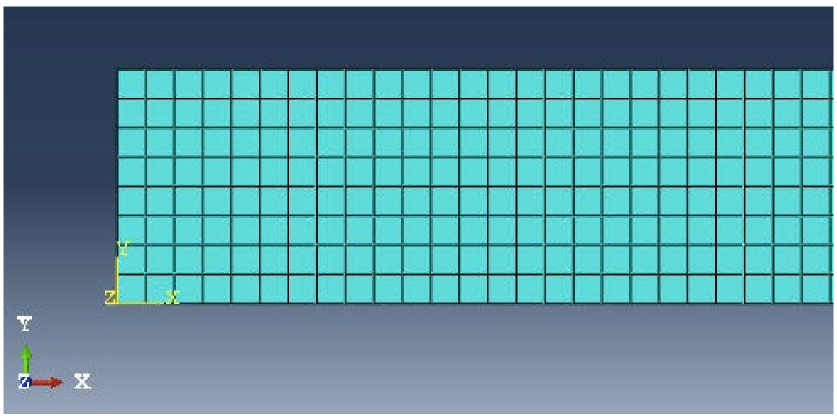

FIGURE 13: MESHED ELEMENTS ON PLATE MODEL

SENSOR PLACEMENT

Waves are received at nine nodes located on the top surface ½ cm apart, as shown in Figure 14. The received signal at a sensor is reported as the displacement as a function of time.

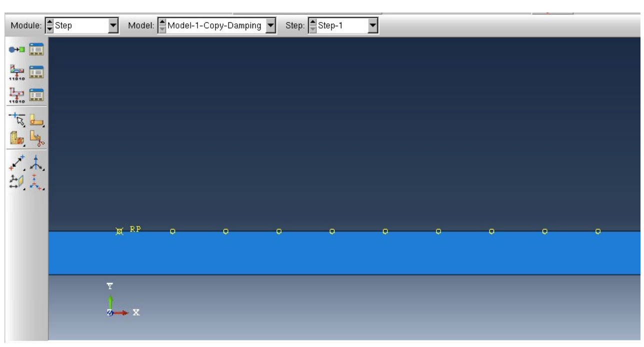

FIGURE 14: SENSOR PLACEMENT ON PLATE MODEL

PIPE

The pipe is composed of the same anisotropic bone material as the plate. Its dimensions are shown in Figure 15.

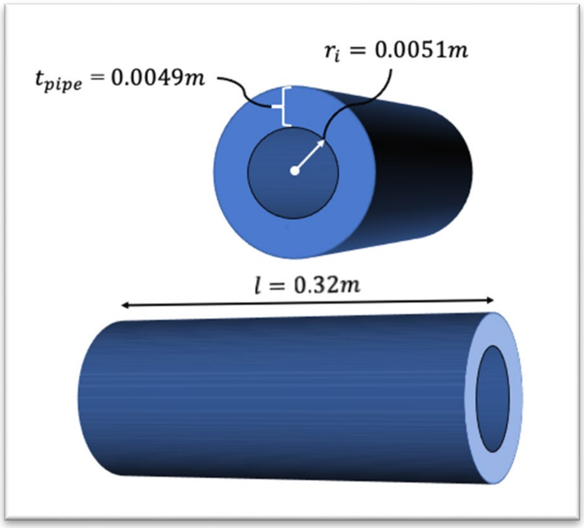

FIGURE 15: PIPE DIMENSIONS

MODEL SIMPLIFICATION AND EXCITATION

The pipe's geometry can be simplified by modeling it symmetrically about the longitudinal axis, shown below in Figure 16. This is known as an axisymmetric model. The ultrasound excitation is represented by the orange arrows and is applied at the bottom of the pipe in the +z direction.

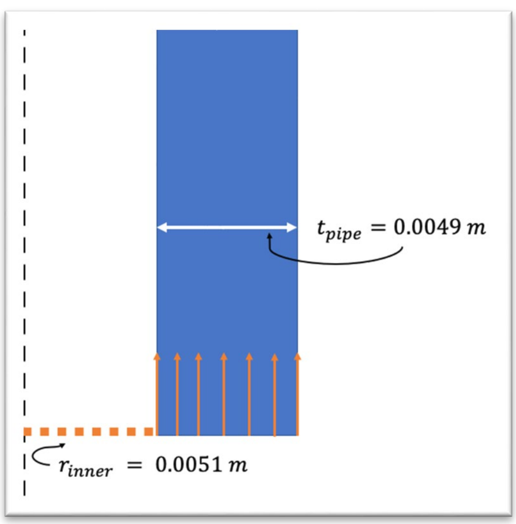

FIGURE 16: AXISYMMETRIC MODEL SIMPLIFICATIONS

MESH

Due to the models' simple geometry, Quadrilateral type elements with 4 nodes are used. The 2D axisymmetric pipe mesh composed of these elements is shown in Figure 17:

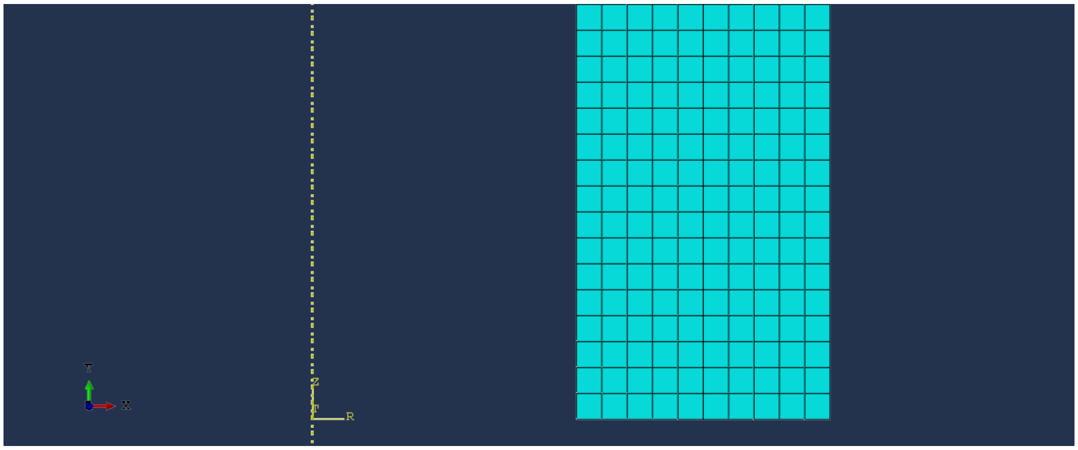

FIGURE 17: 2D AXISYMMETRIC PIPE MESH

Axisymmetry simplifies a 3D model into a 2D one. The 2D model can be meshed and extrapolated to create a 3D mesh of the pipe as seen in Figure 18.

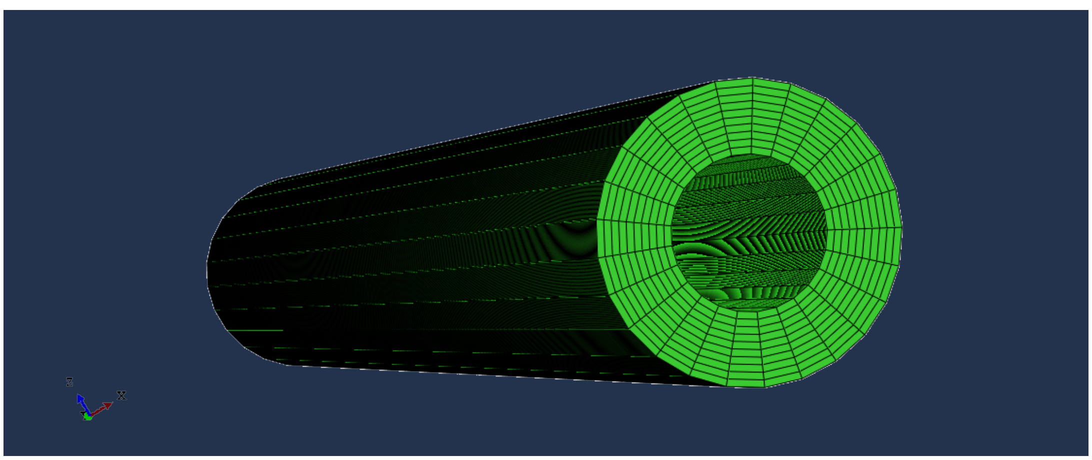

FIGURE 18: 3D MESH OF PIPE

Sensor Placement

As in the plate simulation, sensors will be placed 0.005 m between 0.090 m and 0.135 m along the outer edge of the pipe. This conformation is seen in Figure 19.

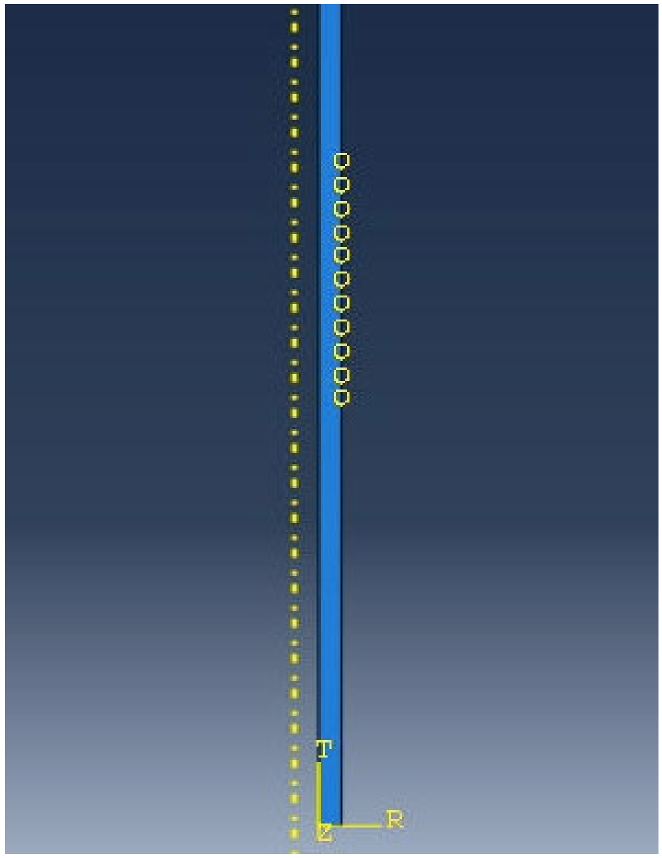

Figure 19: Sensor Placement on Pipe

The sensors are named Sensor Node 1 (SN1) through Sensor Node 10 (SN10) with SN1 being the sensor at 9cm and SN10 at 13.5 cm. Consecutive sensor nodes are ½ cm apart.

In both the plate and the pipe, the guided waves are actuated by dynamic displacement loading applied to the end. The dynamic loadings are 8 cycle Hanning windowed tonebursts with center frequencies of 200 kHz and 500 kHz, shown in Figure 20. This loading is intended to generate the S0 mode in the plate and the L(0,2) mode in the pipe.

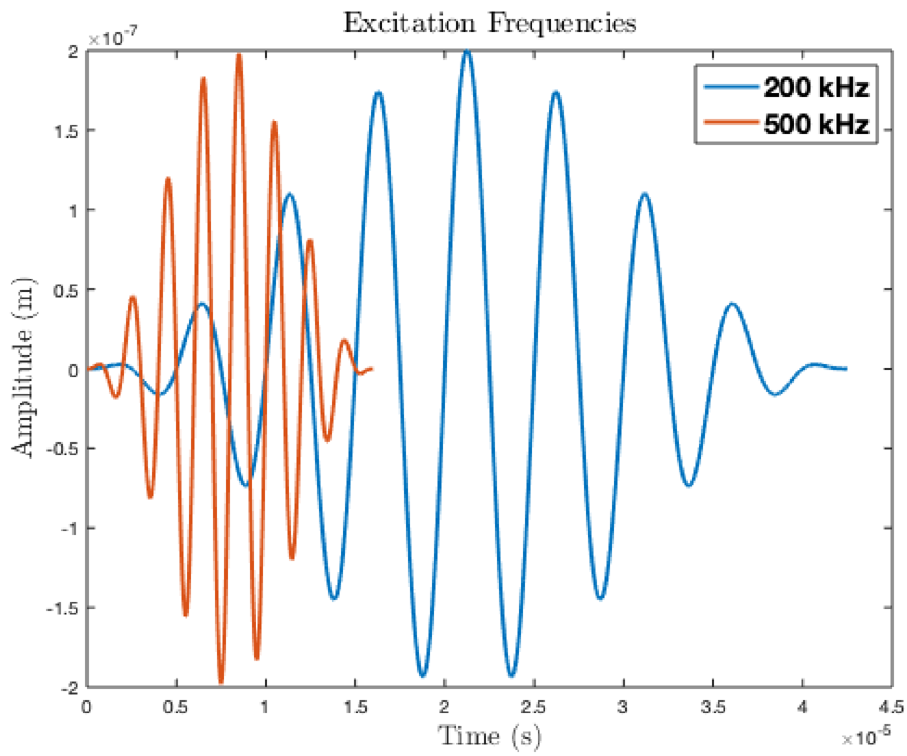

FIGURE 20: 200 AND 500 KHZ EXCITATION LOADINGS

CHAPTER 4
RESULTS

AMPLITUDE DATA

The wave signals from different sensor locations are plotted as a function of time in the following figures. These are the displacement components in the X-direction. This type of plot is known as an A-scan. These results are for the damped pipe and plate.

DAMPED PLATE

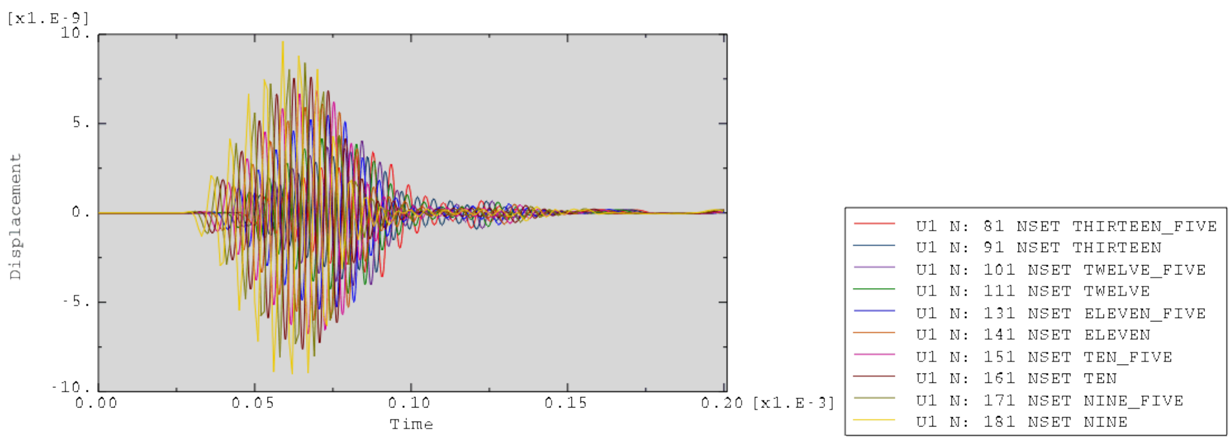

(a)

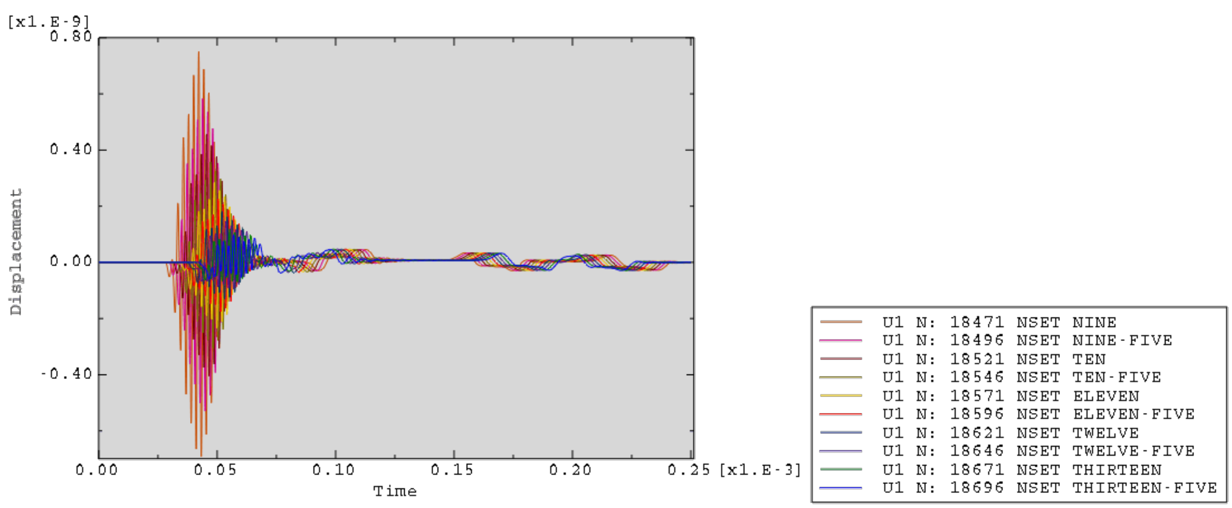

(b)

FIGURE 21: COMPOSITE PLOT OF TRAVELING WAVE FORM FOR (A) 200 KHZ AND (B) 500 KHZ

DAMPED PIPE

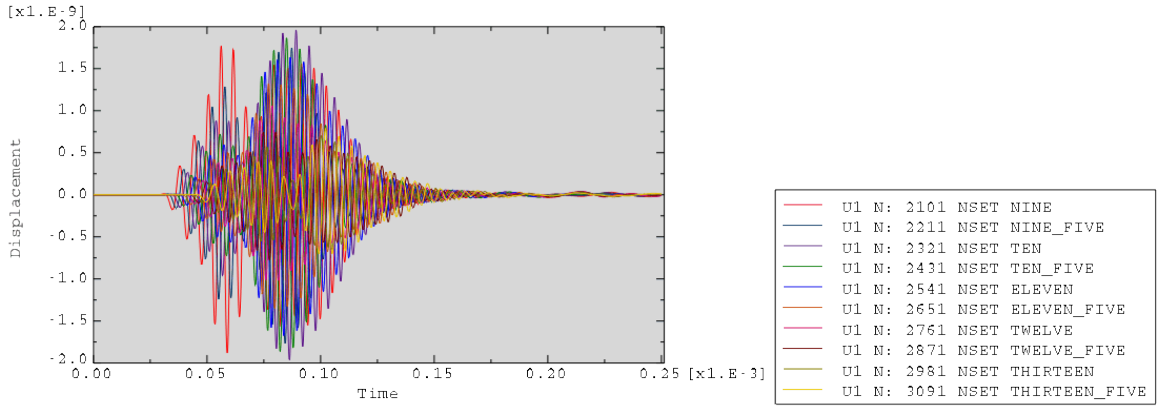

(a)

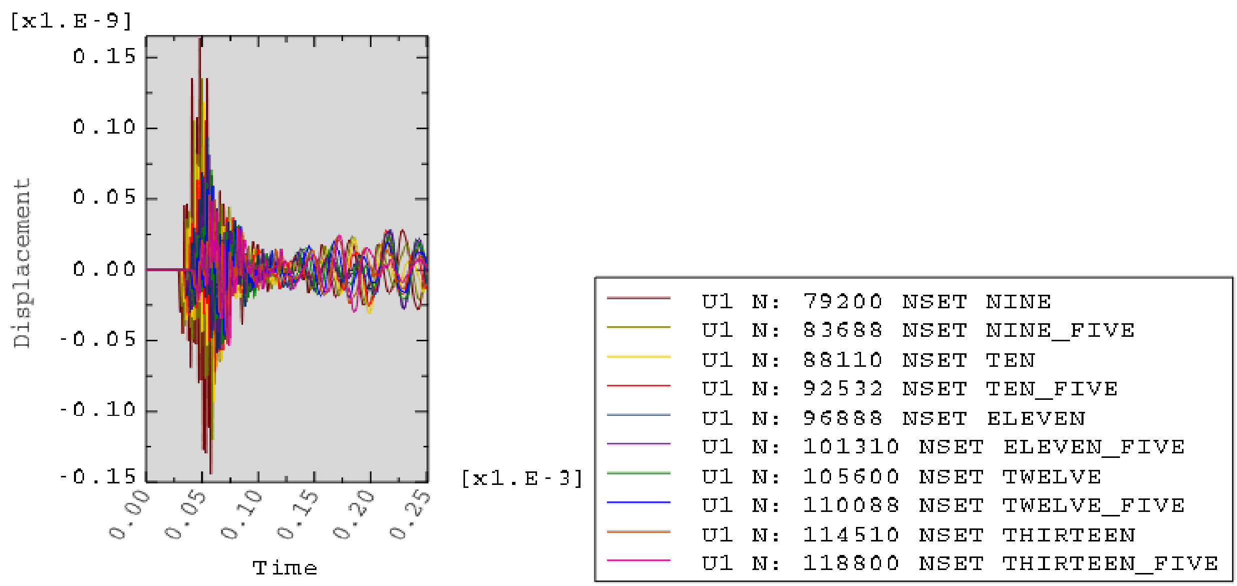

(b)

FIGURE 22: COMPOSITE PLOT OF TRAVELING WAVE FORM FOR (A) 200 KHZ AND (B) 500 KHZ

In Figure 21 (a) and (b) the A-scans have one mode. In Figure 22 (a) the 200 kHz wave propagates as two modes. It is unclear what modes are propagating in Figure 22 (b).

GROUP VELOCITIES

Group velocities are calculated based on a waveform's time of arrival at different points in space. A Hilbert Transform is used to find the waveform's peaks at different points along the waveguide's length.

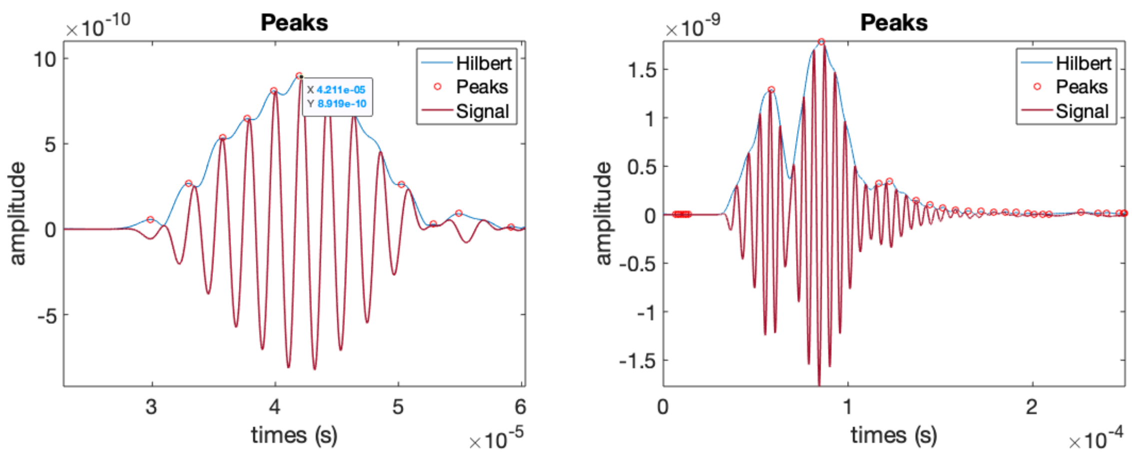

(a) (b)

FIGURE 23: HILBERT TRANSFORM PEAKS FOR (A) SINGLE MODE WAVES AND (B) DOUBLE MODE WAVES

Each of the modes that makes up a wave have a characteristic group velocity. Figure 23 (a) is a waveform with a single mode while Figure 23 (b) is a waveform with two modes.

To calculate group velocity, a Hilbert transform is used to identify the peaks of the wave modes at two sensors, SN1 and SN2, separated by a known distance, Δx. Then the distance between sensors is divided by the time difference, or the time of arrival (TOA), for waveform's peaks to find the group velocity:

$$v_G = \frac{\Delta x}{TOA_2 - TOA_1}$$

EQUATION 4

When more than one mode is present, group velocities for each mode can be calculated and compared to theoretical values. Group velocities calculated for damped models of both waveguides are shown in Table 6 below.

TABLE 6: CALCULATED GROUP VELOCITIES OF DAMPED MODELS

	Group Velocity (km/s)	
	$\mathbf{200}\ \boldsymbol{kHz}$	$\mathbf{500}\ \boldsymbol{kHz}$
Plate	2.318	3.077
Pipe	1.661	inconclusive
	3.067	

Plate Simulations

The U1 displacements for damped and undamped plate simulations are plotted for the first sensor SN1 at 9cm (in green) and the last sensor SN10 at 13.5cm (in blue), shown in Figure 24 and Figure 25, respectively.

200 kHz

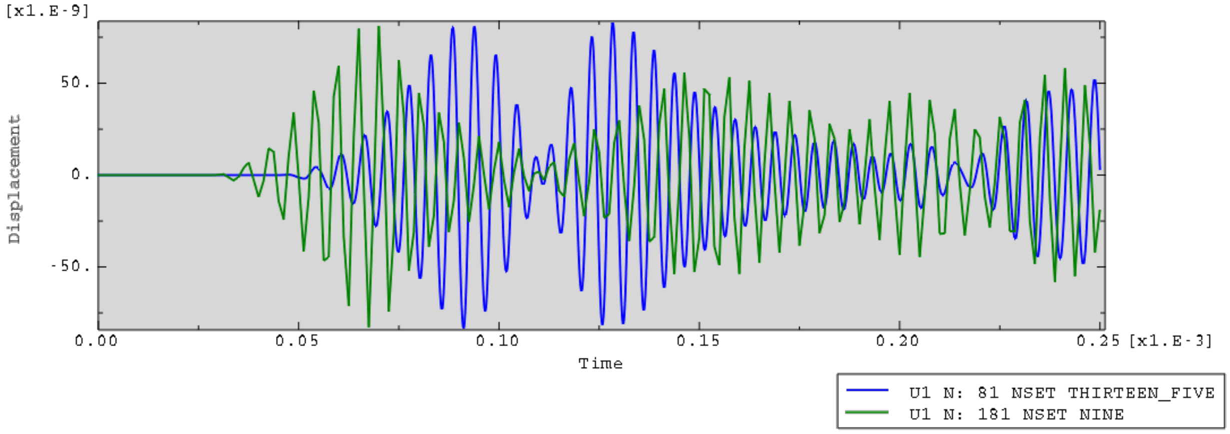

(a)

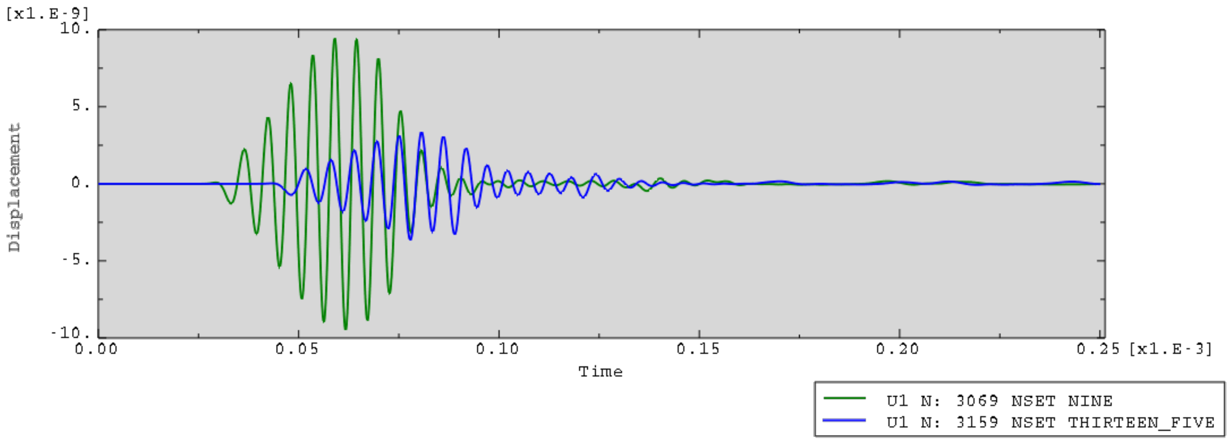

(b)

Figure 24: U1 Displacement At Final Sensor – Plate 200 kHz

(A)Undamped (B) Damped

500 kHz

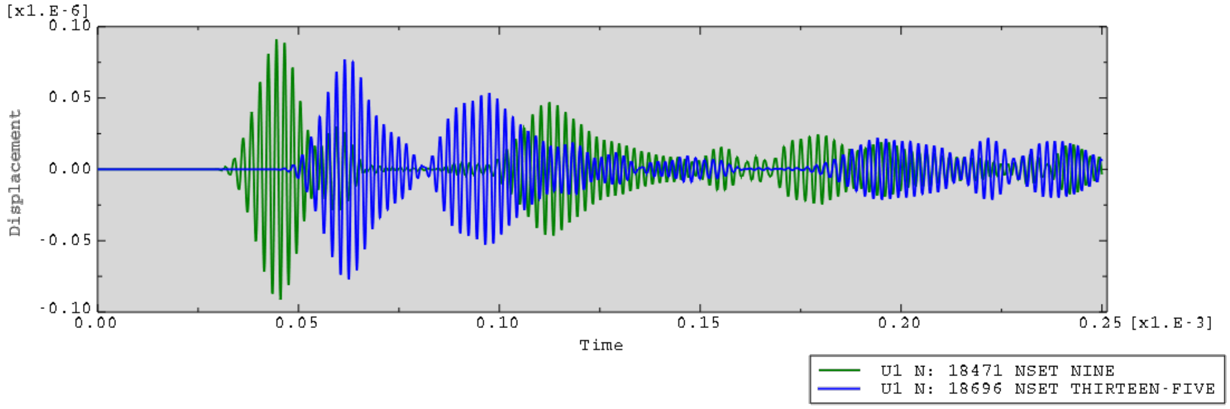

(a)

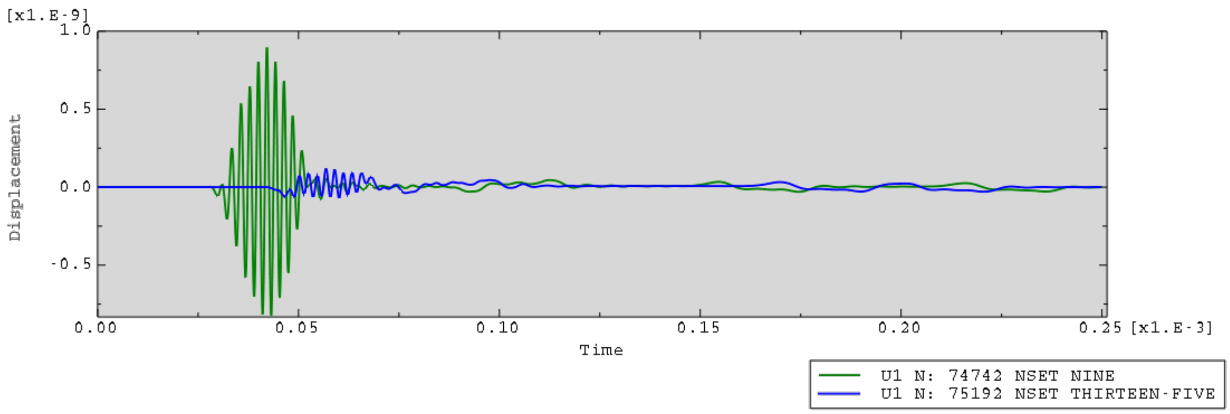

(b)

FIGURE 25: U1 DISPLACEMENT AT FINAL SENSOR – PLATE 500 kHZ

(A) UNDAMPED (B) DAMPED

PIPE SIMULATIONS

The U1 displacements for damped and undamped pipe simulations are plotted for the first sensor SN1 at 9cm (in green) and the last sensor SN10 at 13.5cm (in blue), shown in Figure 26 and Figure 27, respectively.

200 KHZ

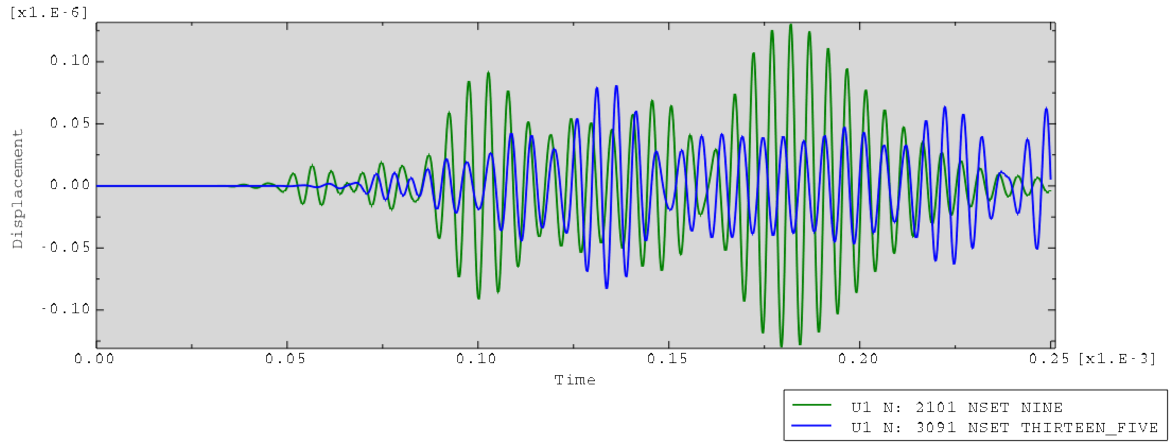

(a)

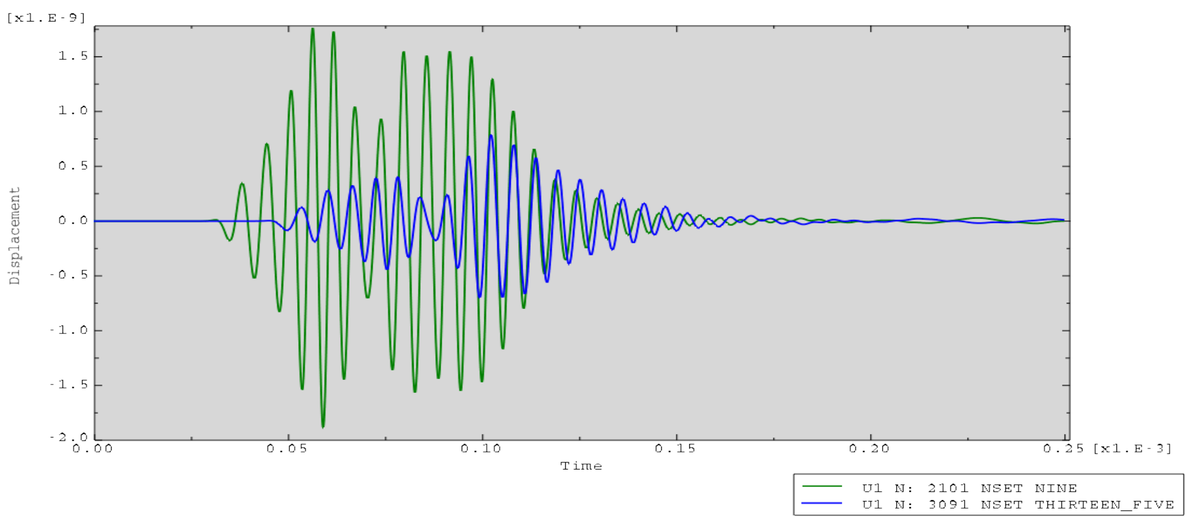

(b)

FIGURE 26: U1 DISPLACEMENT AT SN1 AND SN10– PIPE 200 KHZ

(A) UNDAMPED (B) DAMPED

500 kHz

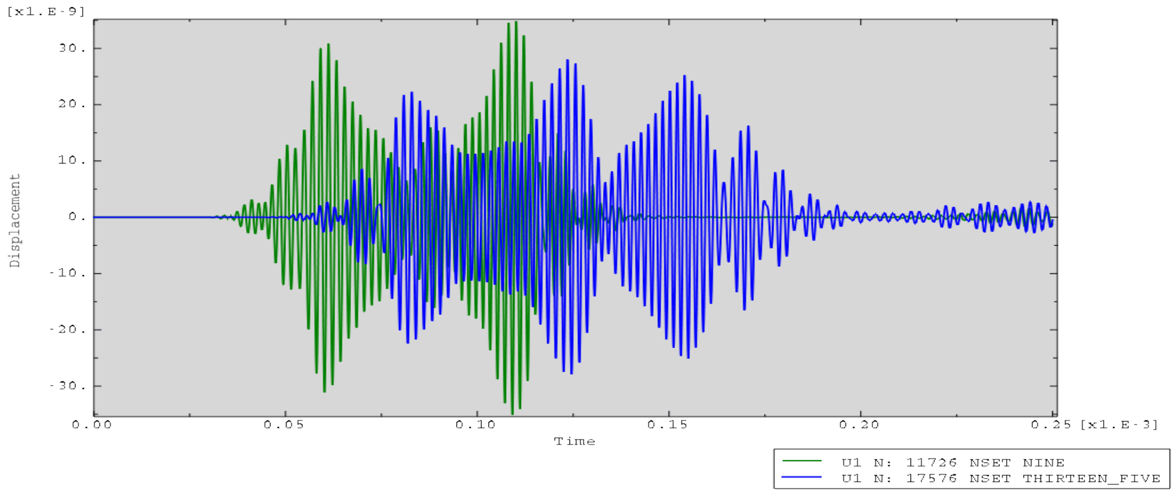

(a)

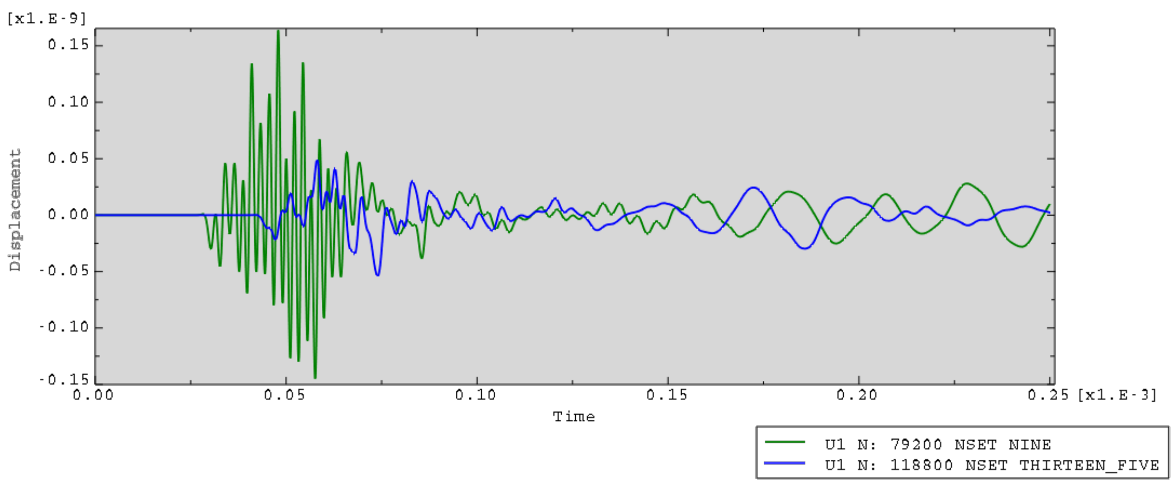

(b)

FIGURE 27: U1 DISPLACEMENT AT SN1 AND SN10– PIPE 500 KHZ

(A) UNDAMPED (B) DAMPED

Amplitude Comparison

The attenuation can be quantified using a damping factor (DF), dividing the peak SN1 amplitude of the undamped simulation by the peak SN1 signal of the damped simulation for a given frequency.

$$DF = \frac{Undamped\ Y_{PeakSN1}}{Damped\ Y_{PeakSN1}}$$

Equation 5

A Hilbert Transform is used again to find the peak amplitudes. For the resulting calculation, a larger factor means greater attenuation. Results are shown in the following table.

Table 7: Amplitude Ratios For $\frac{Undamped}{Damped}$ at SN1

	Amplitude Ratio: $\frac{Undamped}{Damped}$	
	200 kHz	**500 kHz**
Pipe	69.25	215.43
Plate	8.54	102.7

The attenuation factor between 200 and 500 kHz frequencies for the damped models at SN1 is shown in Table 8. A higher number indicates more attenuation in the damped 500 kHz model compared to the damped 200 kHz model.

Table 8: Amplitude Ratios For $\frac{200kHz}{500kHz}$ SN1

	Amplitude Ratio: $\frac{200kHz}{500kHz}$
Pipe	11.5621
Plate	10.6982

CHAPTER 5
DISCUSSION

From Figure 21 (a) and (b), it is clear that ultrasound sent through a damped plate at both frequencies propagates as a single wave mode; an isolated A-scan clearly showing a single mode can be seen in the damped results of Figure 24 (b) and Figure 25 (b). The single mode nature is less clear in the undamped plate A-Scans of Figure 24 (a) and Figure 25 (a) since multiple wave packets can be seen as time progresses in the simulation. These additional amplitudes can be explained by the sensors recording wave reflections from the back wall of the plate. In the damped models, this phenomenon is not present due to the dissipation of the wave's energy before it can reflect back and reach the sensor again.

The single propagation mode for the damped 200 kHz plate simulation has a group velocity of 2.318 km/s. From the theoretical group velocities in

Table 4, this value is close to both the A0 mode (1.9708 km/s) or the SH0 mode (1.968 km/s), but the SH0 mode is unlikely to be actuated by the applied loading.

The A-scans shown in Figure 24 for a 200 kHz pipe excitation display two propagation modes in both the damped and undamped cases. The calculated group velocities for these two modes from Table 6 are 1.661 and 3.067 km/s. Based on the theoretical group velocities contained in

, the mode at 3.067 km/s would have to be the S0 mode. Again, since the theoretical group velocities for A0 and SH0 modes are so close, it would be difficult to say which mode is represented by the 1.661 km/s.

For the 500 kHz excitation, undamped propagation clearly shows the two modes in Figure 28. When damping is applied to the model, there appears to only be one mode. However, measurements made closer to the excitation source revealed two modes.

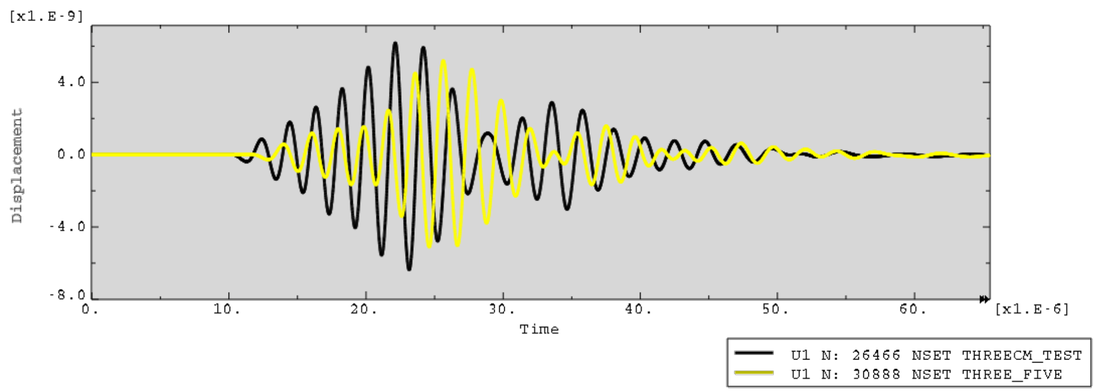

FIGURE 28: DOUBLE MODE PROPAGATION NEAR SOURCE - 500 KHZ PIPE

Complications arise in the calculation of group velocities when there is significant mode mixing in a model. Figure 29 below shows mode mixing in amplitude data for the damped pipe at 500 kHz at various sensing points (note: it is a dynamic figure).

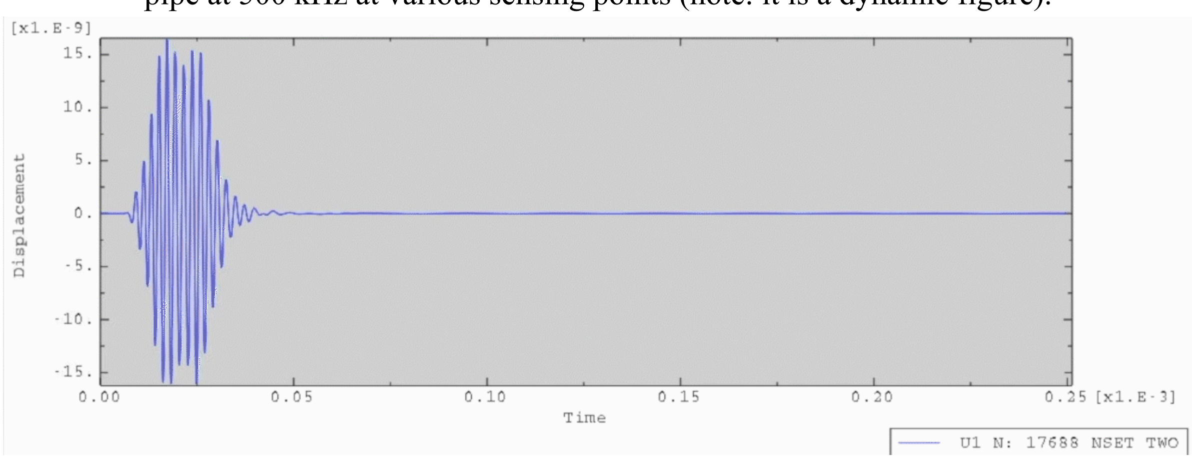

FIGURE 29: MODE MIXING IN 500 KHZ PIPE NEAR SOURCE

These A-scans were made at points starting at 2 cm from the source with 0.5 cm increments. Compared to the distance of 9 cm used for SN1, these measurements are much closer to the source . The first A-scan resembles something close to a single mode, but as the wave propagates it splits two wave packets temporarily then back into something that could neither be classified as a single or double mode wave. For this reason, calculating the group velocity would likely give inaccurate results.

As to be expected, the damping of the material properties decreased displacement amplitude at both frequencies and in both geometries. Table 7 lists attenuation factors at sensor node 1 (SN1) peak amplitudes for undamped versus damped models. A higher attenuation factor correlates with greater decrease in amplitude at SN1 between models.

Based on the damping factor calculations from Table 8, a 500 kHz frequency used as a load for either waveguide will show greater damping than a 200 kHz frequency load on the same waveguides. This indicates that even with the damping constants scaled to have the same effect for each frequency, there exists an intrinsic damping when using 500 kHz waves for an excitement load. The data from Table 7 would also indicate greater signal attenuation in the pipe for both frequencies.

CHAPTER 6
SUMMARY AND CONCLUSION

For the damped 200 kHz pipe, the S0 mode was identified based on group velocity calculations. The other mode was most likely the A0 mode. The damped 200 kHz plate mode present could either be the A0 or the SH0 mode. For the damped 200 kHz pipe two modes with group velocities of 1.661 and 3.067 km/s corresponding to the L(0,2) and L(0,4) modes. Finally, the modes present in a damped 500 kHz pipe could not be accurately calculated due to the highly variable wave packets received. Excitation loadings of 500 kHz experience greater attenuation for the same amount of simulated damping. A 200 kHz signal should be the preferred excitation frequency when receiving waves over longer distances in bone. First, they experience less damping over time by the material, allowing them to travel farther. Second, their A-scan packets are more distinguishable modes. As a waveguide, the pipe causes significantly more attenuation in the signal than the plate. A plate-shaped bone would be a better waveguide than a pipe-shaped bone.

Future Work

A 3D CAD model of the fifth-metatarsal was obtained but due to both time and technical constraints is outside of this paper's scope. Filament was obtained from FibreTuff Inc., a company that specializes in bone-like biomaterial for use in 3D printing. The .STL file was used to print the metatarsal for use in future experiments. Figure 28 shows the .STL file used in printing and the printed bone.

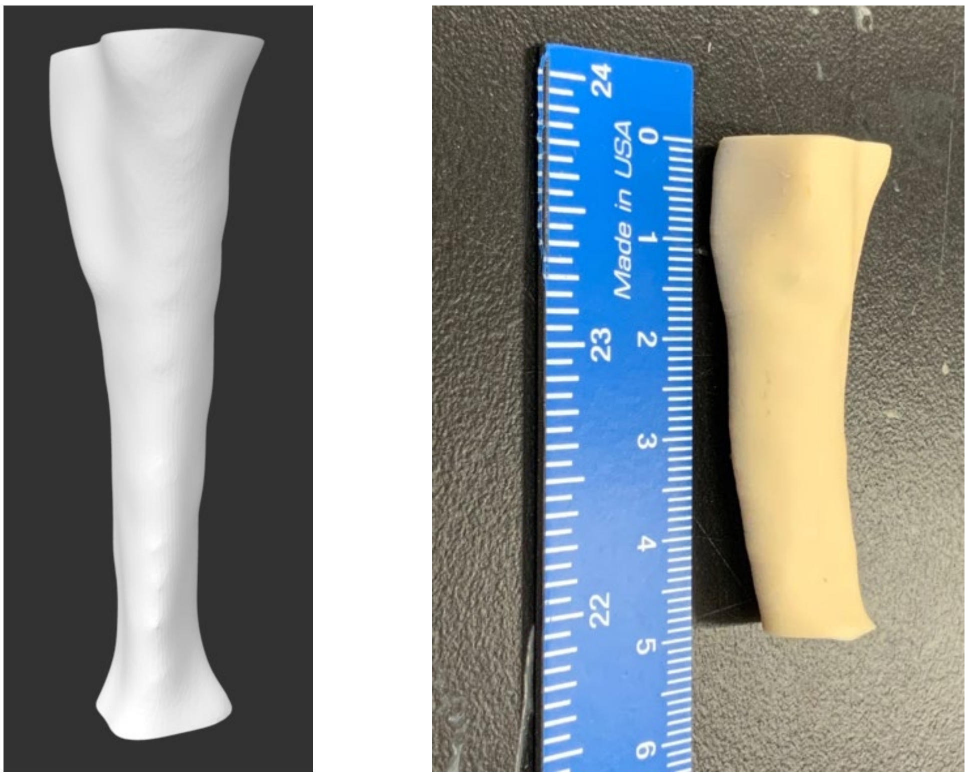

(a) (b)

FIGURE 30: 3D MODEL OF 5TH METATARSAL (A) AND 3D PRINTED MODEL OF 5TH METATARSAL (B)

Using the same procedure of physical experiments confirmed by simulations, the 3D-printed model will be excited with transducers and the metatarsal model from will be used for simulations.

The next step would be to fracture the physical and simulated model, repeating the tests done on the original model. This way, the characteristic response of the wave interacting with a fracture can be obtained.

BIBLIOGRAPHY

1. Hall T. Quantitative Ultrasound: Transition from the Laboratory to the Clinic. In: *APS March Meeting Abstracts*. Vol 2014. APS Meeting Abstracts. ; 2014:Y38.002.

2. Marshburn TH, Legome E, Sargsyan A, et al. Goal-directed ultrasound in the detection of long-bone fractures. *J Trauma - Inj Infect Crit Care*. Published online 2004. doi:10.1097/01.TA.0000088005.35520.CB

3. Krieg MA, Barkmann R, Gonnelli S, et al. Quantitative Ultrasound in the Management of Osteoporosis: The 2007 ISCD Official Positions. *J Clin Densitom*. Published online 2008. doi:10.1016/j.jocd.2007.12.011

4. Bierig SM, Jones A. Accuracy and cost comparison of ultrasound versus alternative imaging modalities, including CT, MR, PET, and angiography. *J Diagnostic Med Sonogr*. Published online 2009. doi:10.1177/8756479309336240

5. Guha A, Aynardi M, Shokouhi P, Lissenden CJ. Material and geometric effects on ultrasonic guided wave propagation in long bones (Conference Presentation). In: ; 2020. doi:10.1117/12.2558582

6. Battaglia PJ, Kaeser MA, Kettner NW. Diagnosis and serial sonography of a proximal fifth metatarsal stress fracture. *J Chiropr Med*. Published online 2013. doi:10.1016/j.jcm.2013.10.002

7. Rose JL. *Ultrasonic Guided Waves in Solid Media*.; 2014. doi:10.1017/CBO9781107273610

8. Modarres M, Amiri M. Probabilistic Structural Health Monitoring. 2015;(June).

9. Cheeke DN. *Fundamentals and Applications of Ultrasonic Waves*. Second.; 2012.

10. MarketsAndMarkets. Ultrasonic Testing Market worth 3.93 Billion USD by 2022. e-Journal of Nondestructive Testing.

11. Protopappas V, Vavva M, Fotiadis D, Malizos K. Ultrasonic monitoring of bone fracture healing. *IEEE Trans Ultrason Ferroelectr Freq Control*. Published online 2008.

doi:10.1109/TUFFC.2008.787

12. Fast Facts About Osteoporosis. American Bone Health. Published 2020. Accessed January 8, 2021. https://americanbonehealth.org/fast-facts/

13. Hans D, Krieg MA. Quantitative ultrasound for the detection and management of osteoporosis. *Salud Publica Mex*. 2009;51(SUPPL.1):25-37. doi:10.1590/S0036-36342009000700006

14. Tibia and Fibula Shaft. Team Bone. Published 2016. https://teambone.com/education/education-clinical/adult-orthopedic-trauma/tibia-and-fibula-shaft/

15. Guha A, Aynardi M, Shokouhi P, Lissenden CJ. Shear-actuation and vibrometer reception of penetrating ultrasonic guided wave modes in human tibia. *Appl Sci*. Published online 2020. doi:10.3390/app10238397

16. Huh J, Easley ME. Surgical Management of Proximal Fifth Metatarsal Fractures. Muscoskeletal Key. https://musculoskeletalkey.com/surgical-management-of-proximal-fifth-metatarsal-fractures/

17. James A. Nunley MD. FRACTURES OF THE BASE OF THE FIFTH METATARSAL: The Jones Fracture. *Orthop Clin North Am*. 2001;32(171-180).

18. Kaufman J, Luo G, Siffert R. Ultrasound simulation in bone. *IEEE Trans Ultrason Ferroelectr Freq Control*. Published online 2008. doi:10.1109/TUFFC.2008.784

19. Belegundu A, Chandrupatla T. *Introduction to Finite Elements in Engineering*. 4th Editio.; 2011.

20. Mathematical Models and Assumption for Anisotropic Mechanical Properties. Moldex3D. Accessed March 10, 2021. http://support.moldex3d.com/r16/en/solutionadd-ons_fiber_reference_mathematicalmodelsandassumptionforanisotropicmechanicalproperties.html

ACADEMIC VITA

COLIN SLAVTCHEFF

(203)-868-9579
colin.slav@gmail.com

SUMMARY

Honors college scholar with a rigorous engineering and research background. Professional roles reflect experience in adapting to multiple industries and technical paradigms. Multiple experiences located overseas in different cultures have hardened adaptability and interpersonal skills.

EDUCATION

Schreyer Honors College, Pennsylvania State University

Engineering Science, B.S. - May, 2021

WORK EXPERIENCE

Thesis Researcher, Ultrasonics Research Group - *State College, PA* *Apr 2020 - Present*

- ➢ Creating simulated bone models in finite element software such as Abaqus and COMSOL
- ➢ Combining simulation results with physical ultrasonics data to more accurately diagnose bone fractures

Data Engineering Intern, 3D Glass Solutions - *Albuquerque, NM* *May 2020 - Aug 2020*

- ➢ Established Defect-Tracking and Data Storage via MATLAB and Excel for semiconductor manufacturing operations
- ➢ Created process parameter visualization tool to optimize manufacturing across all company assets

Antennae Systems Intern, Northrop Grumman - *Baltimore, MD* *Sept 2018 - Dec 2018*

- ➢ Built MATLAB code to process 10,000 KB Antenna Data Packets
- ➢ Tested cutting-edge laser technology to facilitate accurate defect detection

Flavourist Intern, Givaudan Flavour House - *Cranbury, NJ* *Jul 2018 - Aug 2018*

- ➢ Compounded 100+ new flavors as part of customer collaborations

LEADERSHIP EXPERIENCE

Schreyer Leadership Development Seminar - *State College, PA* *Apr 2019*

- ➢ Challenged to react to 8 unique business situations with immediate feedback to optimize interpersonal and negotiating skills

China Immersion Program, Engineering Intern - *Dalian, China* *May 2017 - Aug 2017*

- ➢ Gained operational exposure to cutting-edge engineering facilities from Beijing to Dalian including Ford and Rockwell Automation facilities

Entrepreneurship in Israel - *Tel Aviv, Israel* *Mar 2019*

- ➢ Engaged with top leadership of Israeli start-ups across diverse industries including Fiverr, SodaStream, and other companies

VOLUNTEER EXPERIENCE

Caring for Friends - *Yardley, PA* *Apr 2015 - Present*

- ➢ Participated in weekly meal preparation and delivery for the financially disadvantaged and elderly in the Philadelphia area

Engineers Without Borders, Executive Officer - *State College, PA* *Sept 2016 - May 2018*

- ➢ Created community outreach programs and innovative fundraising events to quickly expand member size and organization capital

Penn State THON - *State College, PA* *Sept 2016 - May 2020*

- ➢ Fundraised and Danced for 46 hours during THON weekend on behalf of Engineers Without Borders to bring awareness to childhood cancer
- ➢ Supported food operations during THON weekend as a Hospitality Committee member

TECHNICAL SKILLS

MATLAB, C, C++
Finite Element Analysis
Adobe Creative Suite
Microsoft Office Suite
Conversational Chinese
Conversational Spanish

PERSONAL INTERESTS

Cooking and Wine
Travel
Running
Camping
Graphic Design